A linear pulse amplifier for space flight applications

M. Lampton[a] and G. Penegor
Space Sciences Laboratory, University of California, Berkeley, California 94720

(Received 20 July 1999; accepted for publication 21 August 1999)

We describe a charge pulse amplifier developed for the medium energy neutral atom experiment aboard the IMAGE geophysical observatory. Its purpose is to receive and amplify event pulses from a large area microchannel plate detector. Its design emphasizes low input impedance ($\sim$20 Ω), good dynamic range ($>$10 000:1), and timing accuracy ($<$1 ns) sufficient for neutral-atom time-of-flight determination in the 1–30 keV energy range. The design is robust and free of adjustments, and is expected to tolerate a space radiation environment in which a 300 krad dose will be accumulated. © *2000 American Institute of Physics.* [S0034-6748(00)00501-3]

I. INTRODUCTION

The medium energy neutral atom (MENA) experiment aboard the IMAGE mission is a group of three detectors and ancillary electronics that measure the angular distribution, speed distribution, and atomic number distribution of fast neutral atoms in space resulting from the charge exchange neutralization of geomagnetically trapped ions (Pollock *et al.*[1]). The three detectors are similar but are aimed in different directions to span an enlarged field of view. Each detector head (Fig. 1) comprises an electrostatic charged particle deflector or broom, a fine pitch transmission grating to exclude ultraviolet (UV) and visible light, a thin foil produce start trigger electrons when an incoming neutral atom enters the instrument, a drift region, and a *Z*-stack triple microchannel plate detector that senses the electrons from the start event and shortly thereafter senses the atom itself (the stop event). Electron cascades from the microchannel plate stack are collected by an array of 100 parallel anode conductors maintained at a positive high voltage (+3400 V) via separate 1 MΩ load resistors. These anode strips are located on the front face of a dielectric anode plate. On its rear surface, position sensing pickup electrodes at ground potential capacitively sense the arrival of charge on the front. They deliver negative charge signals proportional to the microchannel plate (MCP) event size, but divided into two portions that depend on the vertical position of the event, from which the vertical arrival position and angle can be determined.

Science data are obtained from each event in several ways. The amplitude of each start event is employed to determine the electron yield of the foil when the incoming atom arrives; this can be used to infer, within limits, the energy of the atom. The time of occurrence of the start pulse begins the time-of-flight measurement needed for the atom speed determination. The amplitude of the stop event is also an indicator of the atom energy, and the timing of stop ends the time-of-flight determination.

The start event charge is divided into A and B portions whose relative pulse heights are used to infer the vertical position of the start event within the detector aperture. Similarly, the stop event charge is divided into A and B portions to determine the vertical position of the atom's arrival at the MCP. These two determinations are subtracted, giving a measure of the angle at which the atom passed through the detector's drift region, permitting the incident atom direction to be determined in the vertical plane.

The MENA instrument performance requires that the spatial position error is kept below one percent of the full scale position range for both start and stop, and timing jitter be kept below 1 ns for both start and stop. This level of performance is required not just at a single pulse height, but over a wide range of pulse heights. The dynamic range is set by the broad range of electron yield from the foil (1–10 electrons entering the MCP) widened further by the breadth of the MCPs own pulse height distribution. The triple MCP electron multipliers are known to provide gains of about 2×10^7 with good stability and life. Stimulated by start events in the range 1–10 electrons, broadening in the MCP will deliver output events over a wider range, roughly 0.5–15 equivalent input electrons (−1.6 to −48 pC MCP output). The downstream electronics requires positive pulse heights ranging to 7.2 V peak amplitude. This fact sets our target amplifier gain at −0.15 V/pC, and our nominal system threshold at $V_{max}/30$ or 0.25 V, adjustable by remote telecommand.

To achieve accurate position determinations using charge ratios, the system noise level has to be kept low enough that even a minimum height signal is not significantly disturbed in ratio by more than an allowable 1% full width at half maximum (FWHM) error [0.4% root-mean-square (rms)]. Indeed, since additional errors invariably occur from other causes (sampling, dc drift, ADC) the amplifier noise should contribute only a portion of this error. The design of the position sensitive anode structure gives it an output capacitance of about 150 pF for each of the four signal outputs. This is one of several factors governing the system noise level. Part of the design process was to adopt an amplifier topology for which we can expect an output noise level around 0.2% rms of the 0.25 V threshold pulse height, or 0.5 mV rms. The equivalent input charge noise is 3.3 fC rms. This figure was achieved in the present design.

Another important requirement for the MENA system is

[a]Electronic mail: mlampton@SSL.berkeley.edu

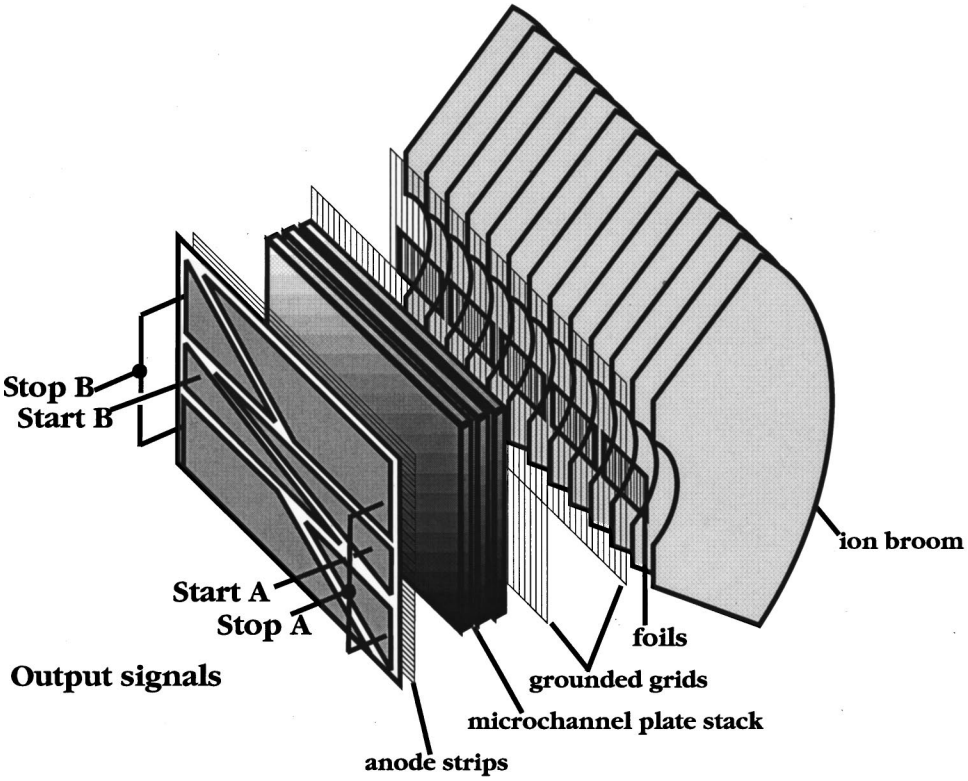

FIG. 1. Diagram of the MENA detector head, illustrating its principal components. An incoming atom enters at the right through the ion rejecting broom. When it passes through the grating/foil assembly it produces a few start electrons whose time and position are sensed on the start electrodes. Later, when the atom itself reaches the MCF, the stop time and position are sensed. The MENA amplifiers receive and amplify the A and B start and stop signals.

to have a very low input impedance for all the charge amplifiers. Because MENA performs start and stop timing on MCP events at differing locations and different times within the same detector, crosstalk is a potentially serious problem. In spite of careful electromagnetic design, the start and stop electrodes within each detector head have a nonzero mutual capacitance of the order of 1 pF. For this reason, charge landing on the start electrodes has to be conducted away quickly, on a time scale much faster than the shaping time constant of the pulse amplifiers, lest start disturb the subsequent stop timing. For this reason we sought to achieve an effective amplifier input resistance no higher than 20 Ω, low enough to give an anode discharge time constant of a few ns, much faster than our adopted pulse shaping time constant.

II. DESIGN OVERVIEW

Our amplifier consists of a front end charge amplifier loop and a rear end shaping amplifier. This architecture derives from a long successful heritage in the field of nuclear spectroscopy. For reviews, see Goulding and Landis[2] or Radeka.[3] The front end loop serves to remove the signal charge from the detector quickly and with a minimum of added noise. It therefore must have a low input impedance and wide bandwidth. The shaper amplifier produces the output pulse wave form. It is basically a filter whose job is to pass the band of frequencies where the signal-to-noise ratio is optimum, while exhibiting an output pulse shape that minimizes pulse pileup.

Before getting into details, let us first consider the broad limitations to be faced in a design of this type. Both the timing performance and the immunity to pulse pileup improve as the pulse shaping time constants are made faster. But, faster pulse shaping means greater bandwidth, which for a given detector capacitance and front end voltage noise density means greater noise. So the first question becomes, how fast can we afford to go, if we are limited only by noise?

When white (flat) amplifier input voltage noise is impressed across a detector capacitance C, the resulting charge noise spectrum is white, and the amount of rms charge noise passed through a linear filter with time constant τ is

$$Q_{\mathrm{rms}} = K_v N_v C/\sqrt{\tau}, \tag{1}$$

where N_v is the rms voltage noise per root Hz. The coefficient K_v is dimensionless and is about 1.0 for all reasonable pulse shapes. Even without further details we can conclude that for a given detector capacitance and noise voltage density, the fastest permissible shaping time constant will be in the neighborhood of

$$\tau_{\mathrm{min}} = N_v^2 C^2/Q_{\mathrm{rms}}^2. \tag{2}$$

For the values $N_v = 1$ nV/root Hz, $C = 300$ pF, $Q_{\mathrm{rms}} = 3$ fC rms, this formula gives 10 ns, suggesting that our final system design must have a shaping time constant of this order or longer.

Beyond signal-to-noise ratio, practical matters can influence the choice of time constants and pulse shape. For MENA, we faced limitations on parts count and amplifier

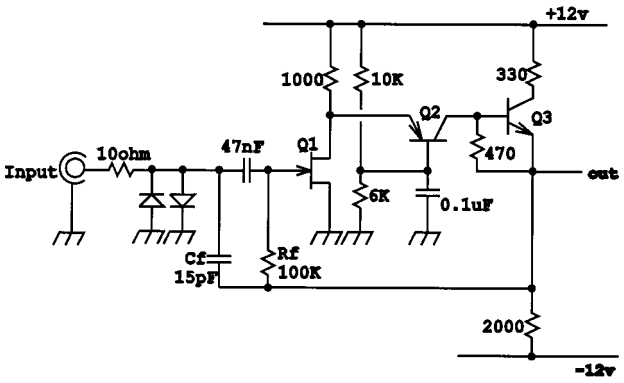

FIG. 2. Schematic diagram of the front end charge loop. The input safety diodes (type 1N4148) serve to protect the active circuits from electrostatic discharge. The other semiconductors are: Q1, IF1801; Q2, JANTX 2N4957; Q3, JANTX 2N2857. Power supply by-passing and filtering components are not shown. Current consumption is 12 mA at +12 V and 6 mA at −12 V.

power consumption, both of which reduce the available gain bandwidth products of the active portions of the circuitry, which would then perform better with longer shaping time constants. More seriously, we faced the issue of crosstalk between the start and stop portions of the anode, and decided that this issue could be best addressed by having a very fast front end response combined with a much slower shaping time constant that would smoothly integrate over the unwanted interfering doublet (bipolar) events while responding fully only to unipolar input charge signals. At the same time, the downstream electronics was being finalized, and we recognized that accurate amplitude sample and hold or peak detector circuits would be much simplified to the extent that the shaping time constant could be lengthened. For these reasons, we adopted the compromise design reported here, which borrows from spectroscopy, where slow pulse shapes are common, and timing, where fast pulse shaping is common.

III. CHARGE AMPLIFIER LOOP

The charge amplifier loop adopted uses an N-channel (JFET) input stage followed by a common base *pnp* cascode load transistor and an *npn* emitter follower, as shown in Fig. 2. This basic design is commonly used in laboratory nuclear spectroscopy (Llacer and Meier;[4] Karlovac and Mayhugh[5]) and has enjoyed a long history of space flight successes, dating back to the original HEAO-1 gas proportional counters and continuing through the EUVE and EURD missions where MCPs are used with charge-division anodes. The field effect transistor (FET) provides very low voltage noise (<1 nV/root Hz) and current noise (<10 fA/root Hz). Its most important role in this circuit is to provide high transconductance so as to keep the closed loop input impedance down. We have chosen the InterFET IF1801 transistor for this application, because it offers a high transconductance at reasonable drain currents (30 mS at 5 mA). The *pnp* transistor serves to provide a low load resistance for the FET to minimize the loss of high frequency gain via the Miller effect within the FET, and to provide a high output impedance for the FET signal current to achieve a large open-loop voltage gain. The *npn* transistor receives this signal and provides current gain to drive the shaping amplifier. The loop is closed by heavy feedback. The feedback capacitor C_f (15 pF) is chosen to be larger than is customary in nuclear spectroscopy applications to accommodate the large signals from the MENA MCP detectors. Also, the heavy feedback allows us to achieve a low closed loop input impedance. We chose an unusually low value of loop feedback resistor R_f (100 kΩ) in order to achieve rapid recovery from overloads and full scale events at high count rates. The feedback resistor contributes a thermal current noise of 400 fA/root Hz that is far greater than the FET alone, and would be unacceptably noisy in a long time constant spectroscopy amplifier. Here, however, its noise contribution is negligible in view of the fast shaping time constant detailed below.

The linear-regime small-signal performance numbers for this three transistor charge loop are largely dependent on a single figure of merit for the loop, namely its radian-gain-bandwidth product (RGBW). Over a broad range of sinewave frequencies, roughly 1 MHz to 1 GHz, the open loop voltage gain varies inversely with frequency, and the product of the voltage gain and the radian frequency is this constant product. Numerically, it is approximately the ratio of the FET transconductance to the sum of the output capacitance of the *pnp* transistor and the input capacitance of the *npn* transistor. In our circuit the transconductance is 0.03 S, the total capacitance is 5 pF, and RGBW is 6×10^9 rad/s.

The input resistance of the closed loop is given by $1/(\mathrm{RGBW}*C_f)$ which is about 10 Ω using our 15 pF feedback capacitor. In addition we interpose a series resistor whose value (10 Ω) is chosen for best damping of the loop response. Connected to a 150 pF detector anode, the charge loop will rapidly drain away the event charge. This small signal time constant is about 3 ns. Equivalently, this time constant can be regarded as a measure of the time needed for the loop to re-establish its input null condition. Let the detector's output capacitance be C_{det} and let the input capacitance of the FET be C_{FET}. Then the total passive capacitance of the input node of the system is $C_{\mathrm{total}}=C_{\mathrm{det}}+C_{\mathrm{FET}}$. The closed loop noise gain of the front end amplifier is C_{total}/C_f, and the closed loop settling time is $C_{\mathrm{total}}/(C_f*\mathrm{RGBW})$.

It is important that this closed loop settling time be brief because it controls interanode crosstalk. This crosstalk is two disturbance currents in rapid succession: a negative current when the electron pulse arrives at its anode, and a positive current while the pulse is drained away through its charge amplifier. The total crosstalk charge in this doublet is zero, but the crosstalk amplifier response is nonzero—indeed, it is proportional to the time duration of this disturbance. Mathematically, the shaper crosstalk output is governed by three factors: the crosstalk attenuation within the anode, the derivative of the nominal (singlet) pulse shape, and the closed-loop settling time. The anode factor is largely fixed by its geometry. The derivative of the pulse shape is largely fixed by our event timing requirements. We therefore depend on minimizing our input-loop settling time to control crosstalk at the amplifier output.

The low frequency performance of the charge loop is also important. At sinewave frequencies below 1 MHz the voltage gain of the charge loop becomes essentially indepen-

dent of frequency. Its value is approximately $VG_0 = g_M * \alpha_2 * \beta_3 * R_{\text{load}}$ where g_m is the FET transconductance, α_2 is the common base current gain of the pnp transistor, β_3 is the common emitter current gain of the npn transistor, and R_{load} is the resistance loading the loop. For our circuit, VG_0 is about 2000. This gain sets the effective low-frequency input capacitance of the charge loop, $C_{\text{eff}} = VG_0 * C_f$. For good long-term accuracy we want to assure ourselves that at least 99% of the pulse signal charge is removed from the anode by the charge loop. We therefore want this effective input capacitance to be at least 100 times larger than C_{total}, or

$$C_{\text{eff}} > 100 * C_{\text{total}} = 25\ \text{nF}. \tag{3}$$

This requirement is met in our design.

The high FET transconductance also helps keep the output impedance of the closed loop charge amplifier circuit very low. The output impedance of the loop is given be $R_{\text{out}} = (C_{\text{total}}/C_f)/(g_m * \beta_3)$ which for our design is approximately 15 Ω. Since the resistance loading the charge loop is about 2000 Ω, the excess gain for this loop is about 40 dB—desirably high from the standpoint of assuring the long term constancy of the closed loop gain upon which the event position calibration relies.

Due to the large size of the full scale input charge signal (−48 pC), the front end loop has to retain its linear behavior over an unusually large range of output voltage swings. A single full scale pulse will give a +3 V edge at the output of the loop. For this reason, front end pileup is a serious concern, explaining our choice of a rather fast (1.5 μs) RC decay time constant for the front end loop.

There is a potentially serious consequence of having so large a nominal swing in our input stage charge amplifier: we are working at peak signal levels that are only 6 dB below the saturation point of transistor $Q2$. If $Q2$ clips, the tight loop null will be briefly lost, and the unnulled input charge will become visible to the other signal channels within the detector. Due to crosstalk this event would be registered as a large amplitude zero time-of-flight event. In the MENA system design we have provided for fixed upper level (UL) discriminators that sense the overload condition at the amplifier outputs and reject all output overloads. For this discriminator to be effective, every front end overload must also trip the UL discriminator. If we had elected to use a very long RC time constant to reset the charge loop as is customary in spectroscopy applications, there would be cases where the front end piles up through a statistical bunching of non-UL events—a circumstance from which we would have no easy recovery. This front-end pileup concern explains our use of an unusually fast RC time constant at this point.

IV. SHAPING AMPLIFIER

The second major element of the amplifier design is the shaping amplifier. It is basically a bandpass filter with gain. Its job is to implement the necessary tradeoff between obtaining good dynamic range (which requires low noise hence narrow bandwidth) and good timing performance (which requires fast response hence wide bandwidth). In addition, with random count arrivals, the response of the shaper must decay quickly after each event to avoid pileup, again favoring wide bandwidth. Because the shaping amplifier controls such a large part of the system characteristics, we present a discussion of the pulse shape considerations before describing our implementation of the pulse shaper.

A. Output pulse shape

For more than 30 years nuclear spectroscopy has motivated efforts to optimize pulse signal-to-noise ratio in the presence of voltage noise, current noise, $1/f$ noise, and microphonic (low frequency) noise. In addition, spectroscopists seek to minimize the loss or confusion of pulse heights for randomly arriving events over a wide range of count rates. Furthermore, large solid state detectors have an intrinsic variation in charge collection time, whose effects need to be minimized in spectroscopy. These considerations have led workers to explore the effectiveness of a variety of pulse shapes. Aspects of the subject have been reviewed by Nowlin and Blankenship,[6] Radeka,[7] Konrad,[8] Nowlin,[9] and Mosher.[10]

We adopted an output pulse shape with several constraints in mind. The output pulse polarity was chosen to be positive, for best compatibility with existing NIM-standard discriminators and pulse height measuring equipment. The shape itself was chosen to be bipolar (positive lobe followed by a negative lobe of comparable amplitude) to give a balanced-area shape having zero dc component, thereby eliminating count rate dependent baseline shifts that would cause errors in the measurement of pulse heights. The bipolar shape has a well defined zero crossing point that provides an accurate walk-free timing feature that can be detected by a zero crossing discriminator. The peak amplitude occurs prior to the zero crossing, which allows a specialized timing discriminator to accept or reject the event on the basis of height prior to enabling the time-of-flight (TOF) subsystem. Of the many possible bipolar pulse shapes, we adopted the double-differentiator double-integrator (DDDI) shape due to its simplicity and immunity to small deviations from the design center circuit parameters.

The one free parameter in the DDDI shape is the choice of time constant τ. This choice affects a number of performance issues. A fast time constant is generally desirable to improve the throughput at high count rates. For example, with random arrivals at 10^4 cps, 1% of all events will be followed within 1 μs by a second event. For any system there is a window of confusion within which two events will be combined and processed as one erroneous event. With the DDDI shape the window of confusion lasts for three time constants. So if we choose $\tau = 0.33$ μs, 1% of the output pulse stream from each amplifier would be erroneous. Considering that a good event needs a clean start and a clean stop, a pileup of 1% per amplifier is a 2% event error rate—a significant limit on the signal-to-noise ratio in the recovered neutral atom images.

We have adopted the value of $\tau = 60$ ns, which is a compromise between minimizing the system noise level and detector crosstalk (which favor a longer time constant) and

minimizing event loss due to pileup (which favors a shorter time constant).

A linear electrical network can be evaluated in the frequency domain, where simple factors incorporate its poles and zeros and yield an algebraic expression for the sinewave frequency response. Since random noise can be decomposed into sinusoids, this frequency response is very useful in evaluating the networks to noise. A linear network can also be evaluated in the time domain to model its pulse response wave form. A comprehensive assessment of amplifier performance needs both analyses.

B. Sinewave response

The sinewave response in the complex frequency domain is completely determined by the locations of its poles and zeros and an overall gain factor. For the DDDI amplifier presented here, the two zeros are at the origin, blocking dc. The four poles are colocated at $\omega = +j/\tau$, where τ is the shaping time constant. To formulate the sinewave gain, first write an input charge signal as a complex sinusoid

$$q(t) = Q_0 \exp(j\omega t) \tag{4}$$

and write the output voltage as another sinusoid

$$v(t) = V_0 \exp(j\omega t). \tag{5}$$

The ratio $V0/Q0$ is the (complex) sinewave charge gain $G(\omega)$

$$G(\omega) = \frac{K_s}{C_f} \frac{(j\omega\tau)^2}{(1+j\omega\tau)^4}. \tag{6}$$

Here, K_s is a dimensionless sinewave gain coefficient. Its value is about -17 in the present design. C_f is the value of the feedback capacitor in the charge loop that is responsible for converting input charge into the voltage drive wave form seen by the shaper. The four poles at $\omega = -j/\tau$ are represented by the denominator. The two zeros at $\omega = 0$ are represented by the numerator.

C. Pulse response

When an event occurs in the microchannel plate, charge is delivered as a brief current signal (a few mA flowing for a few ns). We model the current wave form as an ideal delta function, and the input charge wave form as an ideal step whose height is Q_s. This may be written in the complex frequency domain as

$$Q_{\text{in}}(\omega) = \frac{Q_s}{j\omega}. \tag{7}$$

When this signal representation is applied to the complex gain expression, the resulting product gives the Fourier representation of the output voltage wave form

$$V_{\text{out}}(\omega) = Q_{\text{in}}(\omega) G(\omega). \tag{8}$$

This output signal representation may be converted into its time domain wave form using the Fourier integral. The method of residues is a convenient evaluation method. The result is

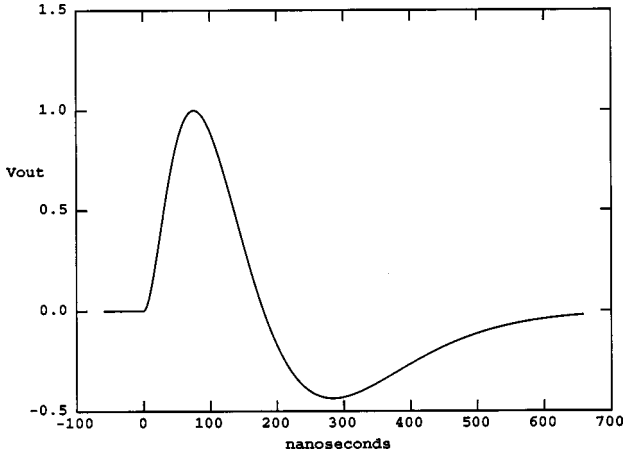

FIG. 3. Theoretical response wave form normalized to make its peak value 1.0. See Eq. (9).

$$V_{\text{out}}(t) = \frac{Q_s K_s}{C_f} \left\{ \frac{1}{2}(t/\tau)^2 - \frac{1}{6}(t/\tau)^3 \right\} \exp(-t/\tau). \tag{9}$$

This pulse (see Fig. 3) initially rises parabolically, controlled by the positive t^2 term. As time proceeds, the negative t^3 term decreases the algebraic part of this expression, and forces a zero crossing at $t = 3\tau$, whereafter the pulse is negative. The overall exponential factor forces the decay of the entire wave form at large *t*. The positive and negative peaks occur at $t/\tau = 3 \pm \sqrt{3}$. For the time dependent part of this expression, the positive peak at $t/\tau = 1.1268$ has a value of 0.1306. The negative peak at $t/\tau = 4.732$ has a value of -0.0569. Because the leading (positive) peak is used to determine the amplitude of each charge event, we characterize the amplifier's charge gain as $V_{\text{out}}(t_{\text{peak}})/Q_s$, or

$$G_{\text{peak}} = 0.1306 \; K_s / C_f. \tag{10}$$

To achieve the desired overall end to end gain of -0.15 V/pC using $C_f = 15$ pF requires that K_s be -17. The minus sign is obtained with a positive shaper gain because the front end loop is an inverter.

D. Amplitude noise

When a broadband noise spectrum is applied to a linear network, the output noise can be computed by integrating that spectrum weighted by the square of the linear network response $G(\omega)$. Two principal noise contributions are commonly encountered in charge amplifier systems: series voltage noise and parallel current noise.

The voltage noise is usually dominated by the input stage FET, amplified by the noise gain of the charge loop and filtered by the network. Let the FET voltage noise spectral density be denoted N_v, independent of frequency. (Typically $N_v \sim 1$ nV/root Hz.) Then the rms voltage at the output of the shaper amplifier will be

$$V_{\text{rms}} = \frac{N_v C_{\text{total}} K_s}{C_f} \sqrt{\left(\int_0^\infty \left| G(\omega) \right|^2 df \right)}. \tag{11}$$

Integrals of this type are best evaluated using beta or gamma function identities

$$\int_0^\infty \frac{x^{2m}dx}{(1+x^2)^{n+m}} = \frac{1}{2}B\left(m+\frac{1}{2}, n-\frac{1}{2}\right) \tag{12}$$

$$= \frac{1}{2}\frac{\Gamma(m+\frac{1}{2})\Gamma(n-\frac{1}{2})}{\Gamma(m+n)} \tag{13}$$

$$= \pi\frac{(2m-1)!!(2n-3)!!}{2^{m+n}(m+n-1)!}. \tag{14}$$

The DDDI network with series voltage noise is the case $m=2$ and $n=2$. The dimensionless integral has the value $\pi/32$. The integral in Eq. (11) thus has the value $1/64\tau$, and the rms output voltage is

$$V_{\rm rms} = \frac{N_v C_{\rm total} K_s}{8C_f\sqrt{\tau}} \tag{15}$$

which is about 130 μV for our amplifier design.

This output noise level can be expressed as an equivalent input charge signal by dividing it by the conversion factor relating peak output voltage to input charge derived above

$$Q_{\rm rms} = K_v\frac{N_v C_{\rm total}}{\sqrt{\tau}}, \tag{16}$$

where the dimensionless coefficient $K_v = 0.957$ for the DDDI shaper. For our circuit this amounts to 1 fC or 6000 electrons rms.

The current noise arises in two ways in charge measuring systems. There is shot noise associated with dc leakage current, and thermal noise from resistors that shunt the input. Both contributions give current noise spectral densities that are essentially flat with respect to frequency. The fact that a charge signal is the time integral of a current signal gives the mean square charge spectra an overall $1/f^2$ behavior. If the current noise density is denoted N_c amperes/root Hz, the amplifier output noise will be

$$V_{\rm rms} = \frac{N_c K_s}{C_f}\sqrt{\left(\int_0^\infty \frac{|G(\omega)|^2}{\omega^2}df\right)}. \tag{17}$$

This integral corresponds to the case $m=1$ and $n=3$, for which the integral has a value $\pi/64$, giving

$$V_{\rm rms} = \frac{N_c K_s\sqrt{\tau}}{8C_f}. \tag{18}$$

In our circuit the dominant current noise contribution is the thermal noise from the 100 kΩ resistor R_f, for which $N_c = \sqrt{(}4kT/R_f$ is 0.4 pA/root Hz. This predicts about 14 μV for our implementation, negligible compared to the voltage noise contribution owing to our shaping time constant being so brief. This output noise term can also be put into the form of an equivalent input charge signal

$$Q_{\rm rms} = K_c N_c\sqrt{\tau}, \tag{19}$$

where the dimensionless coefficient $K_c = 0.954$ again. This charge noise term is 0.1 fC or 600 electrons rms for our amplifier.

There is a third noise source that dominates these front end terms in our low gain design: the shaper amplifier. It is largely due to the voltage noise of our op amp, amplified by its closed loop gain via the feedback path that implements the final pole and zero. The nominal voltage noise density of the op amp (5.5 nV/root Hz) multiplied by the output stage gain and root bandwidth predicts an output noise contribution of about 300 μV rms, in reasonable agreement with our overall measurements. In terms of equivalent input charge, this term is

$$Q_{\rm rms} = 7.66C_f V_{\rm rms}/K_s \tag{20}$$

which evaluates to about 2 fC or 12 500 electrons rms.

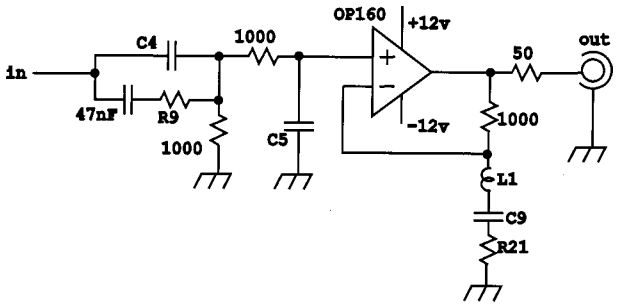

FIG. 4. Schematic diagram of the rear end shaping amplifier. The operational amplifier is type OP-160. C4=68 pF; C5=47 pF; L1=470 nH; C9 =2.2 nF; R21=33 Ω. Power supply by-passing and filtering components are not shown. Current consumption is 7 mA at +12 V and 7 mA at −12 V.

E. Timing noise

To obtain a timing signal that is independent of pulse amplitude we use the zero crossing point of the DDDI wave form. The rms timing error at this point is

$$t_{\rm rms} = V_{\rm rms}/\dot{V}, \tag{21}$$

where $\dot{V}$ is the magnitude of the rate of change of the voltage at its zero crossing point. For the DDDI wave form,

$$\dot{V} = 0.572V_{\rm peak}/\tau \tag{22}$$

and therefore we have

$$t_{\rm rms} = 1.75\tau V_{\rm rms}/V_{\rm peak}. \tag{23}$$

In our system, this amounts to 0.18 ns rms for an event that just barely triggers our lower threshold. It decreases for larger signals.

F. Shaper implementation

To create a pulse shaper that meets our requirements, we combined a passive network and an active feedback amplifier. The circuit is shown in Fig. 4. The passive network is the differentiator formed by the series capacitor C4 and the network resistance. The integrator is the shunt capacitor C5 and the network resistance. Together these give two poles and one zero. We eliminate the slow exponential decay in the charge loop response by applying pole zero cancellation to this first CR differentiator as described by Nowlin and Blankenship[6] via the resistor R9.

The active feedback amplifier comprises the op amp and the damped resonator L1, C9, and R21. This loop contributes two poles and one zero. The op amp is a type OP-160 trans-

resistance amplifer, chosen here for its slew rate (1 V/ns) and its output drive ability (35 mA). It also has a low enough noise level that our overall noise requirement is met, although our design-center gain is so low that the shaper amplifier, rather than the charge amplifier, dominates the output noise. We chose the RLC values for best conformance with the expected pulse shape plotted in Fig. 3.

V. PARTS AND PACKAGING

We packaged two amplifiers into a single housing, these two being the A and B portions of a detector start anode. A separate but identical package contains the A and B amplifiers for the stop anode. We adopted this arrangement because it was extremely important to eliminate any crosstalk between start and stop signals, but not so important to separate A and B signals—these are heavily coupled at the detector anode, and in any case occur at the same time. The circuitry was laid out for production on four-layer boards, with one layer being a continuous ground plane. The two charge amplifier loops are at one end, and the two shapers are at the other. The board measures 38×86 mm. We located a simple resistive attenuator between the front ends and the rear ends to provide a convenient gain set option. To simplify the downstream analog processing, we arranged for one shaper to receive the output of the A preamp, while the other receives the sum of A+B, and is used both for pulse height determination and timing. The A output is used only for position ratio determination.

Each amplifier package includes two test input connectors that are driven by an external rectangular pulse whose height can be set by remote telecommand. The purpose of these test inputs is to permit checking throughout the spacecraft integration process and in orbit. Within the amplifier units, each test input connects to a charge input via a 2 pF capacitor, so that a −5 V transition corresponds to a −10 pC signal which is approximately 20% of full scale.

The aluminum housing and covers are relatively heavy (6 mm thick) to reduce the radiation damage from the orbit environment over the course of a mission lasting two to three years. Empirical radiation dose curves indicate that a 300 krad environment will be attenuated to a level of about 25 krad by this housing, a level tolerated by the component parts. The one thin (2 mm) panel of the housing is its mounting face, which in operation is screwed to the heavy baseplate of the detector rear housing.

The parts selected conform to the provisions of JAN-TX or JAN-TXV for discrete bipolar transistors, and to MIL-STD-883B for the OP-160 microcircuits. The FETs were screened by an independent screening laboratory. The capacitors were chosen from qualified vendors, procured to a specification CCR05CG for the small value ceramic units and CSR13E for the large value solid tantalum capacitors using for filtering and by-passing. Electrical connectors are type DEM-9P for the multiconductor power plug. The coaxial signal connectors are SMA series 9432 from Applied Engineering Products, manufactured to QPL M39012/61 specifications.

Figure 5 is a photograph of two units with their covers removed. One unit shows its topside components, and the other is turned to show its circuit board underside. The aluminum housing and lids are passivated with an alodyne treatment to reduce the possibility of corrosion and to provide a reliable electrical ground path throughout the enclosure, which serves as a shield against electromagnetic interference.

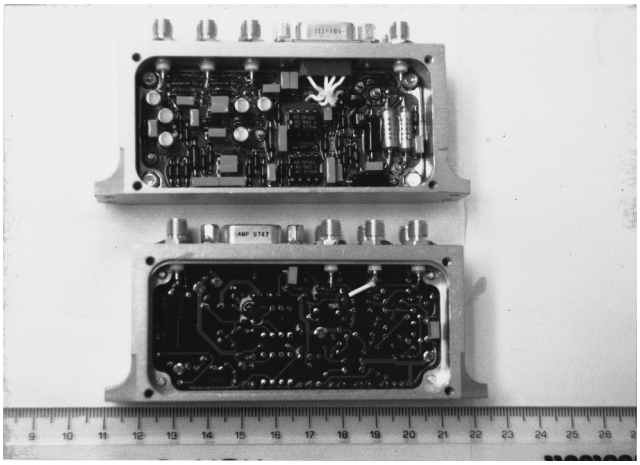

FIG. 5. Photograph of two amplifier assemblies, each of which contains two front end charge amplifiers and two shapers. The coaxial input and output connectors are type SMA. Electrical power is provided via the DEM-9P connector.

VI. PERFORMANCE AND TESTING

A detailed test plan was developed for processing the 14 dual amplifiers produced in support of the MENA project. The overall characteristics are listed in Table I. The electrical tests included the items listed in Table II, plus many hours of operation in vacuum with one or more detector assemblies. Because all amplifiers were found to be virtually identical in performance, their interchangeability during the flight system tests proved valuable. Six of the units have become flight units and are undergoing preflight processing with the other elements of IMAGE/MENA. The preflight test suite includes vibration, electromagnetic susceptibility and emissions, thermal vacuum cycling, and comprehensive calibration and integration tests.

TABLE I. Nominal design characteristics.

Mass (two amplifiers)	179 g
Dimensions (two amplifiers)	11×5×2 cm
Electrical power per amplifier	0.39 W
Charge gain (each amplifier)	−0.15 V/pC
Output voltage swing	+8 V, −4 V bipolar
Output drive capablity	500 Ω load, 16 mA
Shaper time constant T	60 ns
Time to peak	80 ns
Time to zero cross	180 ns
Differential nonlinearity	<0.5%
Noise at output	350 uV rms
Equivalent input noise	2.3 fC rms
Input impedance	20 Ω
Output impedance	50 Ω

TABLE II. Electrical test plan.

dc current consumption, +12 and −12 V
Pulse gain, input unloaded, channel A to channel A
Pulse gain, input unloaded, channel A to channel Sum
Pulse gain, input unloaded, channel B to channel A
Pulse gain, input unloaded, channel B to channel Sum
Pulse gain, input load 150 pF, channel A to channel A
Pulse gain, input load 150 pF, channel A to channel Sum
Pulse gain, input load 150 pF, channel B to channel A
Pulse gain, input load 150 pF, channel B to channel Sum
Pulse shape: Tpeak, channel A to channel A
Pulse shape: Tpeak, channel A to channel Sum
Pulse shape: Tpeak, channel B to channel Sum
Pulse shape: Tzero, channel A to channel A
Pulse shape: Tzero, channel A to channel Sum
Pulse shape: Tzero, channel B to channel Sum
Noise output, inputs unloaded, channel A out
Noise output, inputs unloaded, channel Sum out
Noise output, inputs 150 pF, channel A out
Noise output, inputs 150 pF, channel Sum out
Input null condition, speed and amplitude
Output drive capability, 500 Ω load, 8 V
Overload recovery waveforms, ×10, ×100, ×1000
Gain variation with positive supply voltage
Gain variation with negative supply voltage
Susceptibility to sine and squarewaves on positive supply
Susceptibility to sine and squarewaves on negative supply

VII. ALTERNATIVES

Due to the tight development schedule for this amplifier project, we were unable to explore a number of potentially attractive alternatives. We briefly list those here.

Although the traditional spectroscopy input transistor is a FET, fast timing systems are relatively insensitive to current noise and a bipolar junction radio-frequency (rf) transistor is feasible in spite of its substantial base current shot noise. This subject has been explored by D'Angelo *et al.*[11] with encouraging results. Very high transconductance and bandwidth is available at modest bias current levels, and the bipolar option could lead to reduced power consumption and/or reduced crosstalk. However time did not permit us to explore the issues of loop stability and electrostatic discharge damage threshold for this option.

Hybrid charge amplifier circuits are available from Amptek, eV Products, and InterFET. These are attractive from the packaging standpoint but lack flexibility with regard to circuit options needed to achieve the very low input impedance and large gain bandwidth product that our present application requires.

Because the dominant noise source in the present design is the output amplifier, it is likely the overall noise figure could be improved by redesigning the shaper for less loss in its passive section and less gain in its active section. The chief issue to be addressed for this option would be the stability margin for the active output loop.

The general-purpose DDDI pulse shape is not optimum for amplitude determination nor for timing. Redesigning the LRC portion of the shaper network to move two poles away from the imaginary ω axis and achieve a somewhat higher Q factor would make the positive and negative peaks more nearly equal and would improve the voltage derivative at the zero crossing point, thereby improving the timing accuracy. An issue here is the tolerance of the pulse shape to parameter drift in the shaper components.

Further improvements in timing accuracy and crosstalk rejection could in principle be obtained by adding more poles to the amplifier transfer function, as described by Nowlin[9] and Mosher.[10] For the present application however the added parts count and parts accuracy requirements were unattractive and these options were not pursued.

ACKNOWLEDGMENTS

The authors gratefully acknowledge the support of the MENA principal investigator Craig Pollock and his team at Southwest Research Institute, under Subcontract No. 83820, and the TWINS project under Subcontract No. 999049Q. The authors thank Dr. H. Funsten for suggesting improvements to the manuscript.

[1] C. J. Pollock *et al.*, in *The IMAGE Mission*, edited by J. Burch (Kluwer, Dordrecht, The Netherlands, 1999).
[2] F. S. Goulding and D. A. Landis, IEEE Trans. Nucl. Sci. **NS-25**, 896 (1978).
[3] V. Radeka, Annu. Rev. Nucl. Part. Sci. **38**, 217 (1988).
[4] J. Llacer and D. F. Meier, IEEE Trans. Nucl. Sci. **NS-24**, 317 (1977).
[5] N. Karlovac and T. L. Mayhugh, IEEE Trans. Nucl. Sci. **NS-24**, 327 (1977).
[6] C. H. Nowlin and J. L. Blankenship, Rev. Sci. Instrum. **36**, 1830 (1965).
[7] V. Radeka, IEEE Trans. Nucl. Sci. **NS-15**, 445 (1968).
[8] M. Konrad, IEEE Trans. Nucl. Sci. **NS-15**, 268 (1968).
[9] C. H. Nowlin, IEEE Trans. Nucl. Sci. **NS-17**, 226 (1970).
[10] C. H. Mosher, IEEE Trans. Nucl. Sci. **NS-23**, 226 (1976).
[11] P. D'Angelo, A. Hrisoho, P. Jarron, P. F. Manfredi, and J. Poinsignon, Nucl. Instrum. Methods **193**, 533 (1982).